The Role of Val-265 for Flavin Adenine Dinucleotide (FAD) Binding in Pyruvate Oxidase: FTIR, Kinetic, and Crystallographic Studies on the Enzyme Variant V265A[†,‡]

Georg Wille,*[,§] Michaela Ritter,[||] Manfred S. Weiss,[⊥] Stephan König,[§] Werner Mäntele,[||] and Gerhard Hübner[§]

Institut für Biochemie, Martin-Luther-Universität Halle-Wittenberg, Kurt-Mothes-Strasse 3, 06120 Halle, Germany, EMBL Hamburg Outstation, c/o DESY, Notkestrasse 85, 22603 Hamburg, Germany, and Institut für Biophysik, J. W. Goethe-Universität Frankfurt/Main, Theodor-Stern-Kai 7, Haus 74, 60590 Frankfurt/Main, Germany

Received December 20, 2004; Revised Manuscript Received February 8, 2005

ABSTRACT: In pyruvate oxidase (POX) from *Lactobacillus plantarum*, valine 265 participates in binding the cofactor FAD and is responsible for the strained conformation of its isoalloxazine moiety that is visible in the crystal structure of POX. The contrasting effects of the conservative amino acid exchange V265A on the enzyme's catalytic properties, cofactor affinity, and protein structure were investigated. The most prominent effect of the exchange was observed in the 2.2 Å crystal structure of the mutant POX. While the overall structures of the wild-type and the variant are similar, flavin binding in particular is clearly different. Local disorder at the isoalloxazine binding site prevents modeling of the complete FAD cofactor and two protein loops of the binding site. Only the ADP moiety shows well-defined electron density, indicating an "anchor" function for this part of the molecule. This notion is corroborated by competition experiments where ADP was used to displace FAD from the variant enzyme. Despite the fact that the affinity of FAD binding in the variant is reduced, the catalytic properties are very similar to the wild-type, and the redox potential of the bound flavin is the same for both proteins. The rate of electron transfer toward the flavin during turnover is reduced to one-third compared to the wild-type, but k_{cat} remains unchanged. Redox-triggered FTIR difference spectroscopy of free FAD shows the $\nu(C_{10a}{=}N_1)$ band at 1548 cm^{-1}. In POX-V265A, this band is found at 1538 cm^{-1} and thus shifted less strongly than in wild-type POX where it is found at 1534 cm^{-1}. Taking these observations together, the conservative exchange V265A in POX has a surprisingly small effect on the catalytic properties of the enzyme, whereas the effect on the three-dimensional structure is rather big.

Pyruvate oxidase (POX)[1] from *Lactobacillus plantarum* catalyzes the oxidative decarboxylation of pyruvate, forming CO_2, H_2O_2, and acetyl phosphate in the process (*1*). The enzyme is a homotetramer with 603 amino acid residues per subunit and a total molecular weight of 266 kDa. Its activity depends on the cofactors flavin−adenine−dinucleotide (FAD), thiamin diphosphate (ThDP), and a divalent metal cation (Mg^{2+}/Mn^{2+}). The crystal structure shows the tetramer to be a tightly associated dimer of dimers. Each monomer consists of three domains (CORE-, FAD-, and ThDP-domain) and binds one molecule of FAD, ThDP, and a metal ion (*2*, *3*).

The protein forces the isoalloxazine moiety of FAD into a conformation that is bent about the N_5-N_{10}-axis by 13° (Figure 1). Since the bent conformation resembles the reduced form of the flavin, this can contribute to an elevation of its redox potential (*4*, *5*). Recent studies using redox-triggered FTIR difference spectroscopy (*6*) have shown that the vibrational bands associated with the $\nu(C_{10a}{=}N_1)$ and $\nu(C_{4a}{=}N_5)$ stretch vibration of the POX-bound flavin are significantly shifted toward lower frequencies when compared to the spectrum of the free cofactor. These shifts are not observed in at least two other flavoproteins for which the crystal structures indicate a planar conformation of the flavin, leading to the assumption that the distortion of the isoalloxazine ring is responsible for the shift of vibrational frequencies, corresponding to a loosening of the associated bonds and an elevation of the redox potential. It has been suggested that, in combination with hydrogen bonding, electrostatic interactions, and π-stacking interactions, the cofactor conformation can also be exploited by the apoenzyme to modulate the redox potential (*7*). It is difficult to separate these effects in a protein environment, but studies with sterically hindered flavin model compounds provide some evidence for this suggestion (*8*). Circumstantial evidence comes from X-ray crystal structures in the PDB (*9*): in flavodoxin, the flavin is almost planar in all three redox

[†] This work was supported by the Deutsche Forschungsgemeinschaft and the Fonds der Chemischen Industrie.

[‡] Structure data have been deposited in the Protein Data Bank under the accession code 1Y9D.

* To whom correspondence should be addressed. Phone, +49-(0)345-5524835; fax, +49-(0)345-5527014; e-mail, georg@bc.biochemtech.uni-halle.de.

[§] Martin-Luther-Universität Halle-Wittenberg.

[||] J. W. Goethe-Universität Frankfurt/Main.

[⊥] EMBL Hamburg Outstation.

[1] Abbreviations: FAD, flavin adenine dinucleotide; FMN, flavin mononucleotide; UV−vis, ultraviolet−visible light; IR, infrared; FTIR, Fourier transform infrared; POX, pyruvate oxidase; ThDP, thiamin diphosphate; AMP, adenosine monophosphate; ADP, adenosine diphosphate; ATP, adenosine triphosphate; NAD, nicotinamide adenine dinucleotide; SHE, standard hydrogen electrode.

10.1021/bi047337o CCC: $30.25
Published on Web 03/10/2005

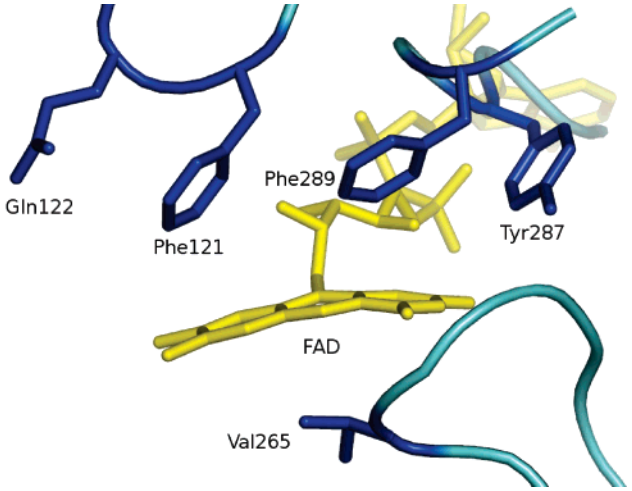

FIGURE 1: The bend of the isoalloxazine ring of FAD in the active site of wild-type POX (*2*). The flavin cofactor is shown in yellow, and residues near both faces of the isoalloxazine ring are depicted in blue.

states (oxidized, semiquinone, and hydroquinone) (*10*, PDB entries 2FX2, 3FX2, 4FX2, 5FX2). In both the oxidized and the reduced form of polyamine oxidase, the flavin is strongly bent (*11*, *12*, PDB entries 1B37, 1H81), and in old yellow enzyme (*13*, PDB entries 1OYA, 1OYC) and thioredoxin reductase (*14*, *15*, PDB entries 1TDE, 1CL0), the oxidized form is planar, while the reduced form is bent.

Pyruvate oxidase hence provides the possibility to address the following questions: first, is the bent conformation of the flavin cofactor responsible for the band shifts in the IR difference spectrum of POX, and second, does the bending contribute to an elevated redox potential of FAD bound to POX as compared to the free cofactor? To this end, we generated the enzyme variant POX-V265A. This conservative exchange reduces the volume of the residue contacting the isoalloxazine ring from below by two methyl groups. The valine acts as a backstop underneath the N_5-N_{10}-axis on the *re* face of the isoalloxazine, with bulky aromatic residues (Phe121, Tyr287, and Phe289) on the opposite face forcing the normally planar moiety to bend along this axis by about 13°. If this backstop is reduced in size, the steric strain is relieved by flattening of the molecule (Figure 1). A closely related question is that of flavin binding affinity. As a shifted redox potential of a bound versus a free cofactor is thermodynamically equivalent to a different affinity of the apoprotein to each redox state, a change of redox potential upon mutation should be reflected in the binding properties of the cofactor.

MATERIALS AND METHODS

Adenine nucleotides, NAD, and ThDP were purchased from Sigma Aldrich; FAD was from AppliChem. Commercially available enzymes and substances were used without further purification.

Site-Directed Mutagenesis. The plasmid pBP200 carrying the wild-type *pox* gene of *L. plantarum* under the control of a *tac* promoter and conferring ampicillin resistance was a kind gift from Prof. R. Rudolph. Mutagenesis of the *pox* gene to obtain the V265A variant from the wild-type was carried out with the QuikChange site-directed mutagenesis kit (Stratagene) according to the instructions of the manufacturer. The primers used had the sequences 5′-GGG-TTC-TGC-TAA-TCG-*CGC*-GGC-ACA-AAA-ACC-GGC-G-3′ and 5′-CGC-CGG-TTT-TTG-TGC-C*GC*-*G*CG-ATT-AGC-AGA-ACC-C-3′. The mutated positions are in italic font. These primers also introduced a silent mutation creating a BstUI recognition site to allow quick first-round screening for successful mutagenesis using a restriction endonuclease digestion. Candidate clones were sequenced in the region of interest to confirm correct incorporation of the exchanged nucleotides.

Protein Expression and Purification. Wild-type pyruvate oxidase and variant V265A were expressed and purified as previously described (*6*).

Stopped-Flow Measurements and Protein Spectroscopy. Rapid kinetics measurements were carried out with an Applied Photophysics SX18 MV stopped-flow spectrophotometer. For the aerobic measurements, one syringe of the device was filled with an air-saturated solution of variant pyruvate oxidase (protein concentration of 8.65 mg/mL in 200 mM potassium phosphate buffer, pH 6.0, and 5 mM ThDP/$MgCl_2$) and brought to reaction with an equal volume of substrate solution (sodium pyruvate of several concentrations in 200 mM potassium phosphate buffer, pH 6.0, air-saturated) through rapid mixing. The absorbance of the protein-bound flavin was monitored at a wavelength of 457 nm (optical path length 10 mm). Kinetic traces were analyzed according to Gibson et al. (*16*). For anaerobic measurements, the experimental setup was the same, and oxygen depletion was achieved with the glucose oxidase method. To each milliliter of POX or pyruvate solution, 5 μL of a glucose oxidase/catalase mixture (~100 mg/mL glucose oxidase, 10 mg/mL catalase in 200 mM potassium phosphate buffer, pH 6.0) and 5 μL of 1 M glucose in H_2O were added.

Conventional protein UV−vis spectroscopy was carried out at 25 °C using an Uvikon 941 spectrophotometer (Kontron). For the dilution experiment, a concentrated solution of POX-V265A (c_p = 113 mg/mL) in 200 mM potassium phosphate buffer and 5 mM ThDP/$MgCl_2$ was diluted with the same buffer in a stepwise manner; that is, to 1 aliquot of the previous concentration sample, 0.5 aliquot of buffer was added. After each dilution step, a spectrum was recorded when no further change in the spectrum was detectable (~15 min). Spectra were measured in quartz cuvettes of either 1 or 10 mm optical path length and corrected for buffer contribution. Competition experiments with AMP, ADP, ATP, and NAD were carried out by adding increasing amounts (max 7 μL) of a 200 mM aqueous competitor stock solution (adjusted to pH 6.0) to an aliquot of 70 μL of POX-V265A (c_p = 15 mg/mL in 200 mM KPP, pH 6.0, and 5 mM ThDP/$MgCl_2$) in a reduced quartz cuvette. Spectra were measured after equilibration (max ~30 min) and corrected for background and for the error introduced by the dilution.

Sample Preparation for Spectroelectrochemistry. Protein samples were prepared by buffer exchange and by concentration of the protein solution to about 1−3 mM bound FAD (i.e., active sites, equivalent to c_p ~ 60−180 mg/mL) using Microcon (Amicon) centrifugation devices. The buffer used for the protein solution was 100 mM potassium phosphate, pH 6.0, and 50 mM potassium chloride. The final flowthrough of the centrifugation devices was clear buffer, in contrast to the bright yellow protein solution, indicating that the amount

of free FAD was negligible. Spectra of free FAD were obtained from a 10 mM solution in 100 mM potassium phosphate, pH 6.0, and 50 mM potassium chloride.

Electrochemistry. The electrochemical IR cell was used as previously described (*17*). The surface of the gold grid working electrode was chemically modified by a 2 mM cysteamine solution. A mixture of redox mediators (for composition see ref *18*, except diethyl-3-methylparaphenylenediamine and dimethylparaphenylenediamine but adding quinhydrone, final concentration of each component ~40 μM) was added to the protein solution prior to its application to the cell in order to accelerate the redox reaction. The cell was then filled with 6−10 μL of protein solution ($c_p \sim 130$ mg/mL), and the path length was adjusted to 6−8 μm. The temperature of the sample cell was kept at 15 °C during measurements. Quoted electrochemical potentials refer to an Ag/AgCl/3 M KCl reference electrode, which are +208 mV below potentials against the standard hydrogen electrode.

Spectroscopy. A modified IFS 25 FTIR spectrometer (Bruker) was used allowing the simultaneous acquisition of IR spectra between 2000 and 1000 cm^{-1} and of vis spectra between 400 and 800 nm as a function of the redox potential applied to the cell. The sample was equilibrated with an initial potential at the working electrode, and a single beam spectrum was obtained. The potential was then changed to its final value, and the sample was allowed to equilibrate. Completion of this process was checked by monitoring the electrode current and by acquiring successive spectra until no further change was found. A second IR and vis spectrum was then measured, and the difference spectrum was calculated with the initial spectrum as reference. For acquisition of IR spectra, 128 interferograms at 4 cm^{-1} resolution were added and Fourier-transformed using triangular apodization and a zero filling factor of 2.

Crystallization. POX-V265A crystals were grown in hanging drops using the vapor diffusion method against a reservoir solution containing 2 M ammonium sulfate. A total of 6 μL of a protein solution ($c_p = 10-15$ mg/mL) in 50 mM phosphate, 20 mM citrate, pH 5.2 (adjusted with NaOH), 5% sorbitol, 10 mM ThDP, 10 mM $MgSO_4$, and 5 mM FAD was mixed with 1 μL of reservoir solution. The drops were streak-seeded immediately and allowed to equilibrate against reservoir solution for 2−8 weeks at 6 °C in the dark.

Data Collection and Processing. X-ray data were collected at beamline X13, European Molecular Biology Laboratory outstation, Deutsches Elektronensynchrotron, Hamburg, Germany. Crystals were flash-frozen in a 100 K nitrogen stream after short incubation in a cryosolution containing crystallization buffer with 2 M ammonium sulfate and 20% glycerol. Diffraction data were processed and scaled with the HKL program suite (*19*).

Crystallographic Model Building and Refinement. Initial phase information was obtained with the structure of wild-type POX (*2*, PDB entry 1POW) as the search model for molecular replacement using the program MOLREP (*20*). Inspection of the electron density and manual model building was done with the program O (*21*). Refinement was carried out using REFMAC (*22*). MOLREP and REFMAC are part of the CCP4 program package, version 5 (*23*). Figures were prepared with PyMOL (*24*). The refined model and structure factors have been deposited in the protein database with the accession code 1Y9D.

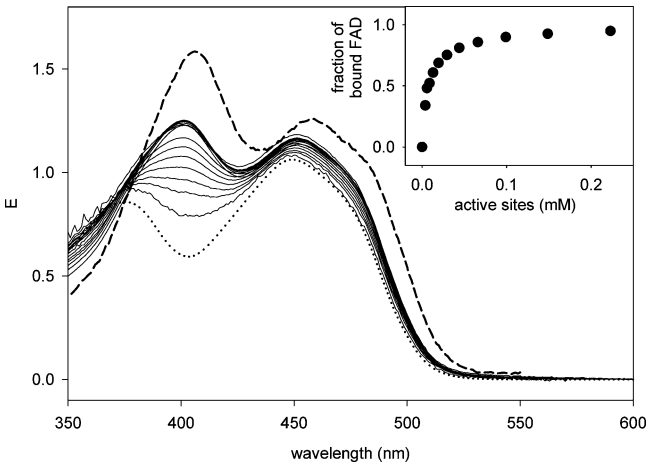

FIGURE 2: The vis spectra of POX-V265A ($d = 1$ mm) at different concentrations (solid lines, c_p ranging from 1.7 mM to 3.8 μM active sites, corresponding to 113−0.25 mg/mL of protein, from upper to lower spectrum, buffer is 200 mM potassium phosphate, pH 6.0, and 5 mM ThDP/$MgCl_2$), corrected for the dilution factor. The dotted line is the spectrum at "infinite" dilution; it is identical to that of FAD. The dashed line gives a spectrum of POX-WT for comparison. Inset: fraction of bound FAD in a dilution series of POX-V265A (in 200 mM potassium phosphate, pH 6.0, and 5 mM ThDP/$MgCl_2$) as derived from the vis spectra.

RESULTS AND DISCUSSION

Spectral and FAD Binding Properties of POX-V265A. FAD shows a significant change in the visible light spectrum upon binding to the apoenzyme of POX-WT, which can be conveniently exploited to monitor the binding process. A similar effect was observed here with the variant V265A, albeit to a lesser extent. Whereas the ratio E_{406nm}/E_{457nm} is about 1.26 for the wild-type POX, it is only 1.04 in the case of the variant. More importantly, the shape of the variant's spectrum is dependent on the protein concentration and is shifted toward the spectrum of free FAD in more dilute solutions (Figure 2). This already indicates that the cofactor is less tightly bound in the variant than in the wild-type, where this behavior is not observed. The analysis of a dilution series of the variant V265A yields a $K_d = 13$ μM. Small-angle X-ray scattering shows the enzyme to still be in the tetrameric state at a concentration of 1 mg/mL, confirming that the release of FAD is not due to the dissociation of the protein's quarternary structure (data not shown). The K_d value for the wild-type POX is difficult to determine precisely and has been estimated to be ≤10 nM (*25*). Therefore, the mutation causes an increase of the dissociation constant by at least 3 orders of magnitude.

Kinetic Properties of POX-V265A. Figure 3 shows the stopped-flow traces of POX-V265A during its reaction with pyruvate under aerobic and anaerobic conditions. At the wavelength of 457 nm used in these measurements, the absorbance due to the enzyme-bound flavin can be monitored, which changes depending on its oxidation state. As for the wild-type, the same reaction observed at 600 nm gave no indication for the intermediate population of a flavin semiquinone species (data not shown). From the turnover in the presence of oxygen, we can calculate a k_{cat} of 15.5 ± 1.3 s^{-1} according to the method of Gibson et al. (*16*), which is almost identical to the value of 16 ± 2 s^{-1} obtained under the same conditions for the wild-type protein (*26*). Usage of the program DYNAFIT (*27*) for a global fit of the traces

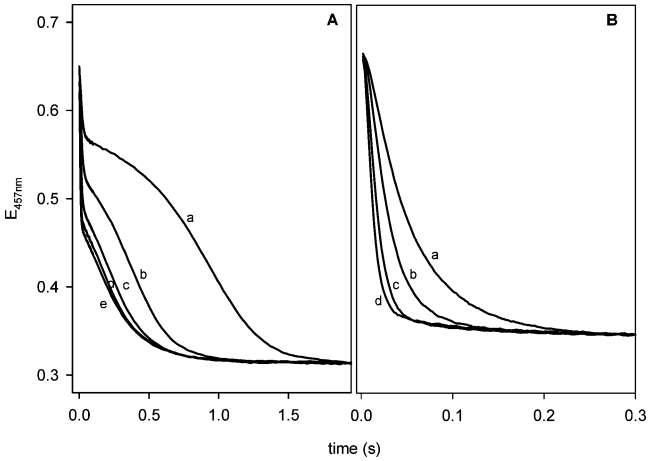

FIGURE 3: Absorbance change at 457 nm of a solution of POX-V265A (c_p = 4.3 mg/mL after mixing) upon rapid 1:1 mixing with different concentrations of pyruvate (concentrations after mixing are (a) 0.5 mM, (b) 1 mM, (c) 2.5 mM, (d) 10 mM, and (e) 25 mM). Panel A (aerobic conditions), solutions were prepared in air-saturated 200 mM potassium phosphate buffer, pH 6.0, and 5 mM ThDP/$MgCl_2$. The decrease in absorbance at 457 nm represents the decreasing ratio of FAD vs $FADH_2$ in the steady state when oxygen is being depleted in the sample cell during turnover. Panel B (anaerobic conditions), solutions were prepared in 200 mM potassium phosphate buffer, pH 6.0, and 5 mM ThDP/$MgCl_2$ and depleted of oxygen with glucose/glucose oxidase/catalase. The decrease in absorbance at 457 nm represents the reduction of FAD to $FADH_2$ during single turnover with pyruvate.

obtained with different concentrations of pyruvate in the absence of oxygen and thus of the reductive half-reaction only yields a rate constant of 130 s^{-1} for the electron transfer from the hydroxyethyl-ThDP carbanion/enamin to the flavin. This is only one-third of the rate of 422 s^{-1} measured for the wild-type (*26*), but since the electron transfer is far from rate limiting for either protein, the overall effect on k_{cat} is negligible.

The reduced rate constant for the electron transfer is an indication that indeed the flavin moiety has different properties in the protein variant.

IR Spectra and Redox Potentials. Redox-triggered difference FTIR spectroscopy was employed to study the effect of the amino acid exchange V265A on the binding of FAD to POX. FTIR spectra of a POX-V265A solution in the oxidized and reduced state were subtracted to give the difference spectrum, revealing a highly detailed "snapshot" of the protein redox transition. Some of the bands can be assigned to certain vibrational modes of the isoalloxazine moiety of FAD. A comparison of the FTIR spectra of POX-WT, POX-V265A, and free FAD is shown in Figure 4, together with the respective vis difference spectra acquired simultaneously in Figure 5. The differences between the IR spectra of POX-WT and FAD have been discussed elsewhere (*6*), the main result being that there is a significant shift of the prominent $\nu(C_{10a}{=}N_1)$ band from 1548 cm^{-1} in free FAD to 1534 cm^{-1} in POX-WT. This band shift was not observed in glucose oxidase or D-amino acid oxidase, and we have attributed the shift to the bent conformation of the flavin in POX. When the two IR spectra of POX-WT and POX-V265A are compared here, it is apparent that they are similar in general but with some significant differences in the region between 1500 and 1700 cm^{-1}. The $\nu(C_{10a}{=}N_1)$ band in the variant is likewise shifted but less so (10 cm^{-1}) than in the

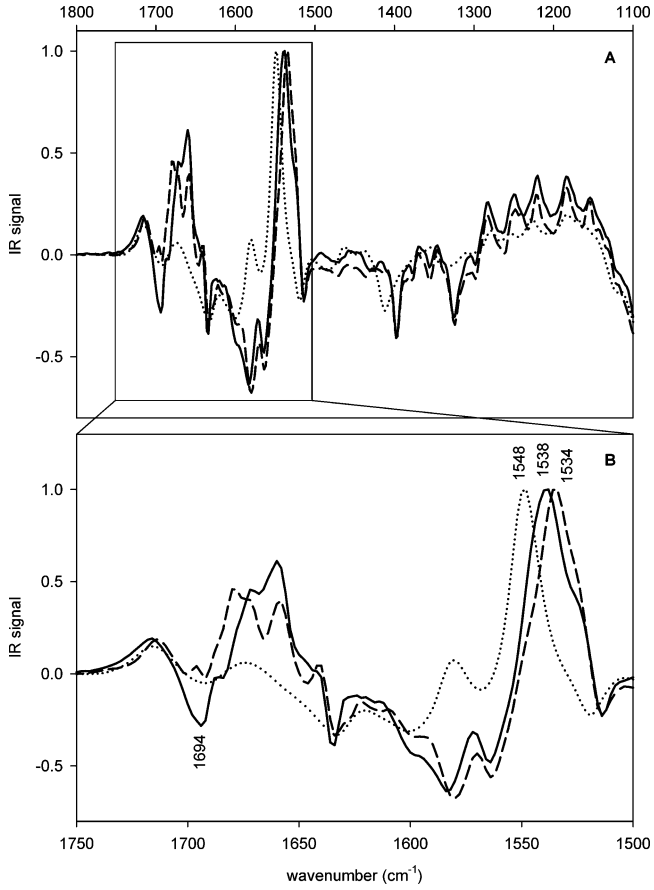

FIGURE 4: (A) Normalized FTIR difference spectra of POX-V265A (solid line), POX-WT (dashed line), and FAD (dotted line) for the potential step from 0.2 to −0.6 V (vs Ag/AgCl/3 M KCl) in 100 mM phosphate buffer, pH 6.0, and 50 mM KCl. (B) Enlarged view of the part of the spectrum that shows the greatest differences between POX-WT and POX-V265A.

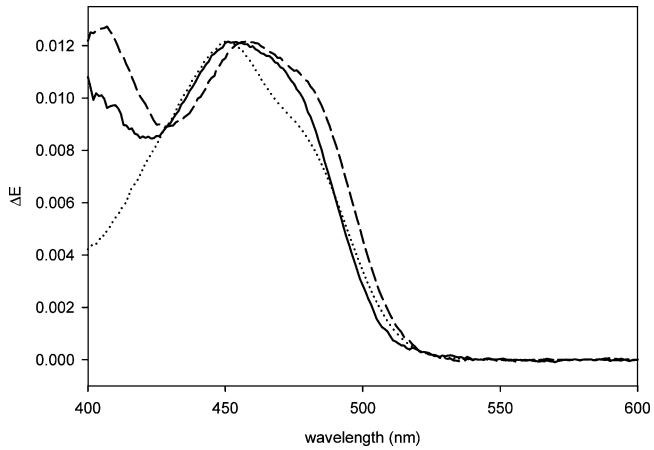

FIGURE 5: Normalized vis difference spectra of POX-V265A (solid line), POX-WT (dashed line), and FAD (dotted line) for the potential step from 0.2 to −0.6 V (vs Ag/AgCl/3 M KCl) in 100 mM phosphate buffer, pH 6.0, and 50 mM KCl.

wild-type, resulting in a peak at 1538 cm^{-1}. This agrees with the assumption that in the variant the flavin is bound in a more relaxed mode than in the wild-type, thereby yielding an IR spectrum shifted more toward that of free FAD. Other difference peaks are found around 1694 and 1670 cm^{-1}, which have no counterpart in either POX-WT or free FAD. Both are consistent with the IR absorption of a glutamine side chain (*28*). A likely candidate would be Gln122, found

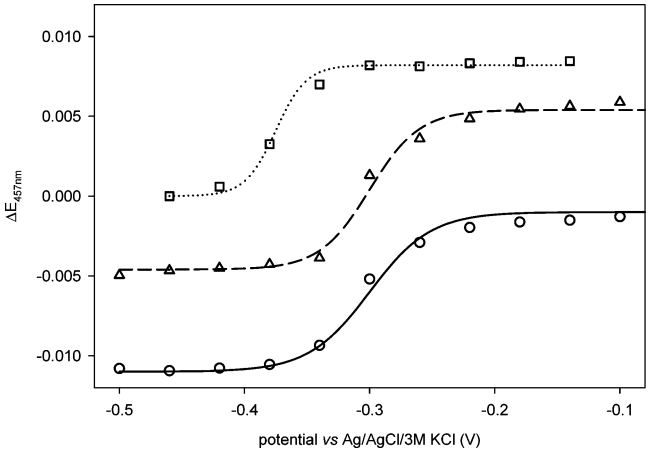

FIGURE 6: Redox titration curves of POX-V265A (solid line), POX-WT (dashed lines), and FAD (dotted line) in 100 mM potassium phosphate, pH 6.0, and 50 mM KCl, following the change of absorbance at 457 nm upon variation of the redox potential in the sample cell. To avoid overlaps, the curves are shifted along the ordinate axis.

near the isoalloxazine in the wild-type structure (Figure 1). As detailed below, this residue is part of a loop that is flexible in the structure of the oxidized variant. It is feasible that the environment of this residue changes upon flavin reduction, for example, rendering the loop more rigid and thus accounting for the spectral changes during the redox transition.

When the redox transition in the electrochemical cell is performed in a stepwise fashion, the resulting spectra, both FTIR and vis, can be used to determine the redox potential of the enzyme. This was done for FAD, POX-WT, and POX-V265A, monitoring the absorbance at the peak wavelength around 450 nm in their respective vis spectra. The result is shown in Figure 6. The calculated midpoint potential for the free cofactor is −375 mV (vs Ag/AgCl/3 M KCl) in good agreement with literature data (*29*). Surprisingly *both* wild-type and variant enzyme yield the same elevated redox potential of −300 mV, corresponding to an increase by about 75 mV versus free FAD. This result, however, is in agreement with the finding that the catalytic properties of wild-type and the variant enzyme are very similar. Within experimental error, the same midpoint potential was obtained independently for POX-WT using the dye titration method (−80 mV vs SHE, equaling −288 mV vs Ag/AgCl/3 M KCl; Tittmann, personal communication). We conclude that even if there are differences in cofactor binding, as evidenced by the decreased binding affinity and the differences in the IR spectrum, they do not affect the redox potential of the bound FAD and change the catalytic properties only slightly. Also, since the redox potential of the bound flavin, a thermodynamic parameter, remains unchanged, the 3-fold rate decrease for the electron transfer observed with anaerobic stopped-flow measurements must be due to kinetic effects.

Crystal Structure of POX-V265A. We determined the crystal structure of POX-V265A to elucidate the structural basis for the discrepancy between the two findings that FAD is bound less tightly and in a different manner in the variant, yet causes only slight changes in the catalytic properties of the enzyme. Data collection and structure refinement statistics are given in Table 1.

Table 1: Data Collection and Model Building Statistics for POX-V265A[a]

space group	$P2_1$, 1 tetramer/au
unit cell	94.66 × 155.78 × 100.75 Å^3, $\beta = 92.92°$
mosaicity	0.475°
no. reflections	581204
no. unique reflections	147399
redundancy	3.94
I/σ	20.6 (2.3)
completeness	99.7% (100%)
R_{merge}	6.2% (64.5%)
R_{rim}	7.2% (75.0%)
R_{pim}	3.6% (37.7%)
resolution	27.3−2.2 Å (2.26−2.2 Å)
no. reflections	147016 (10828)
no. reflections (working set)	139647 (10271)
no. reflections (test set)	7369 (557)
R	17.8% (23.4%)
R_{free}	23.8% (30.8%)
no. atoms in model	19404 (solvent: 1848)
no. ligands	2 × Na^+, 4 × (Mg^{2+}, ThDP, FAD, SO_4^{2-})
rmsd bond lengths	0.018 Å
rmsd bond angles	1.677°
residues in the Ramachandran plot	
most favored	90.4%
additionally allowed	8.8%
generously allowed	0.5%
disallowed	0.3%

[a] Numbers in parentheses refer to the highest resolution shell (2.20−2.26 Å). R_{rim} (redundancy-independent merging R-factor) and R_{pim} (precision-indicating merging R-factor) are defined according to ref *30*: $R_{rim} = (\sum_{hkl}\sqrt{N/(N-1)}\sum_i|I_i(hkl) - \overline{I(hkl)}|)/(\sum_{hkl}\sum_i I_i(hkl))$ and $R_{pim} = (\sum_{hkl}\sqrt{1/(N-1)}\sum_i|I_i(hkl) - \overline{I(hkl)}|)/(\sum_{hkl}\sum_i I_i(hkl))$.

The crystal form obtained for the variant is different from all three previously described forms of the wild-type (*3*). It belongs to space group $P2_1$ with one enzyme tetramer per asymmetric unit. Despite the change in space group, the structure of POX-V265A shows a close overall similarity to the wild-type protein with an rms deviation of just 0.73 Å for the best fit of the protein backbone of the two tetramers (2242 atoms). For the best fit of single monomers, this number is even smaller with only 0.57 Å (558 atoms).

One stretch of amino acids (residues 183−191) is poorly defined in all four subunits. This stretch is part of a long straight segment of amino acid residues connecting the N-terminal core domain and the central FAD domain. While in the wild-type this disorder has not been observed, a similar finding has been reported, for example, for indolepyruvate decarboxylase, another ThDP-containing enzyme with a fold very similar to POX (*31*).

The cofactor ThDP is bound in a nearly identical fashion in both protein species. This is not surprising, considering the almost unchanged catalytic activity of the variant. One feature that could be discerned much more clearly in the new structure of the variant than in the wild-type is the presence of electron density close to the reactive C2-carbon of ThDP. This can be accounted for very well by a tetrahedral oxoanion like sulfate or phosphate (Figure 7). A distinction between these two cannot be made, as both are constituents of the crystallization setup. Because of the higher concentration of sulfate, the ion has been modeled as such. However, since phosphate plays a crucial role in catalysis both as a substrate and as an activating agent for ThDP (*32*) and since

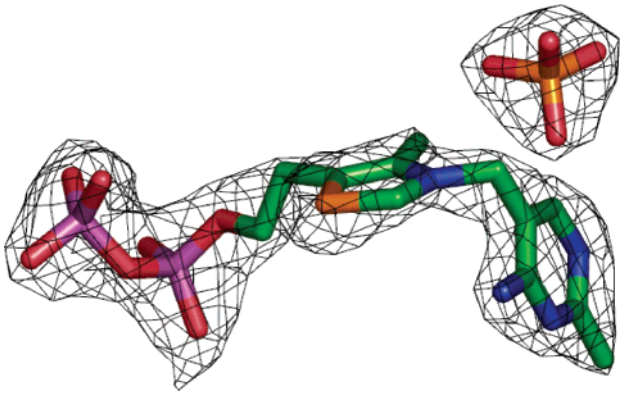

FIGURE 7: The ThDP cofactor in the variant enzyme. Well-defined electron density (σ-level 2.0 in a $2F_o - F_c$ map) above and between the C2-carbon of the thiazolium ring and the N4′-amino group of the pyrimidine ring was modeled as a sulfate ion and could indicate the binding site for the substrate phosphate.

sulfate is neither a substrate nor a competitive inhibitor, it is tempting to speculate that the position of the oxoanion is the phosphate binding site. In wild-type POX, less well-defined additional electron density was found in a similar place and eventually modeled as glycerol, but this can be excluded in our case with confidence.

By far, the greatest differences between POX-V265A and wild-type are apparent in the vicinity of the FAD. Whereas the cofactor is well defined in the wild-type, in the variant, we observe electron density only for the adenosine diphosphate part of the molecule. Interpretable electron density is lacking for the isoalloxazine-ribityl (i.e., riboflavin) moiety as well as for two protein loops comprising part of the FAD binding pocket (residues 116−122, 287−297 with some slight variation between subunits). These loops contain the bulky aromatic residues Phe121, Tyr287, and Phe289 which are involved in the strained binding of the flavin ring (Figure 8A). Interestingly, the loop containing the exchanged residue 265 could be traced in the electron density, albeit with higher temperature factors, and Ala265 is visible (Figure 8B). While amino acid positions at the end of this region superimpose with the wild-type structure, its central part including position 265 shows a greater deviation, having moved further inward into the isoalloxazine binding cavity.

The ill-defined electron density of flavin-binding loops and the isoalloxazine ring itself is a strong indication of disorder and high flexibility in this region of the enzyme, which supports the FTIR spectroscopic observations and leads to the conclusion that the oxidized flavin cannot be strained as much as in the wild-type. The bend of the isoalloxazine in wild-type POX is therefore not responsible for the elevated redox potential compared to free FAD. It should be noted that the situation is very similar in all four subunits of the variant protein structure, which are not related by crystallographic symmetry. This argues against the possibility of a crystallographic artifact. We also rule out that the isoalloxazine-ribityl moiety is physically cleaved off from the ADP, since the crystals retain their bright yellow color and enzyme solutions are stable and active over the same periods as required for crystallization. Furthermore, spontaneous hydrolytic cleavage would be expected to occur predominantly at the phosphoric acid anhydride bond between the phosphates and not at the ester bond with the sugar.

If the isoalloxazine ring is as relaxed as the crystal structure indicates, how can we explain the peak shift for the $\nu(C_{10a}{=}N_1)$ vibration, which is still considerable (10 cm^{-1})? Figure 8C suggests an explanation: residual electron density can be seen near the carbonyl groups of the isoalloxazine, indicating that this part of the cofactor is still fixed in place and acts as a hinge around which the rest of the ring moves. These hydrogen bonds are present in the wild-type and still persist in the enzyme variant; they may well contribute to a loosening of the $C_{10a}{=}N_1$ bond by lowering its electron density. Consequently, this means that the peak shift in wild-type POX is also caused, at least partly, by hydrogen bonding interactions, extending the original explanation involving steric strain (*6*).

The electron density of the adenosine diphosphate part of the FAD is well-defined in the variant, but its position differs from the wild-type. The adenosine moiety is retracted away from the second cofactor ThDP by about 1 Å (Figure 8C). The phosphate linked to the ribose is offset from its position in the wild-type by 1 Å and has lost the hydrogen bond to His101 as the imidazole side chain is rotated by ~90° about the $C_\alpha{-}C_\beta$-axis. However, the terminal phosphate of the ADP, which would be connected to the ribityl moiety of FAD, is only minimally displaced from its corresponding position in the wild-type.

Binding of ADP. The peculiar high mobility of the riboflavin moiety together with the well-defined electron density of the adenosine diphosphate part suggested that the latter serves as an anchor for the cofactor, with the redox-active riboflavin part contributing only weakly to the binding. We hence set up an experiment where we added adenine nucleotides (AMP, ADP, and ATP) to a solution of POX-V265A. The spectral differences between protein-bound and free FAD allowed us to monitor the release of the cofactor in the presence of increasing amounts of competing molecules. We found that indeed all three adenosine phosphates can displace FAD, with ADP and ATP being more effective competitors than AMP ($K_{i,AMP} \sim 3$ mM, $K_{i,ADP} \sim 1.5$ mM, $K_{i,ATP} \sim 1.5$ mM, as estimated from the spectral changes upon addition of varying amounts of competitor). The example of ADP is given in Figure 9.

It is even possible to displace the POX-bound FAD with increasing amounts of NAD despite this cofactor's different shape ($K_i \sim 6$ mM). However, after addition of pyruvate, no trace of the reduced form NADH could be detected.

For comparison, the ADP displacement experiment was repeated with wild-type POX and yielded no measurable effect.

How can the two findings be reconciled that the POX variant V265A binds FAD much more weakly than the wild-type and mostly by means of the ADP anchor, and yet the redox potential of the variant remains virtually unchanged? Thermodynamically, the redox potential is determined by the ratio of the affinity of the protein to the oxidized and the reduced form of the cofactor. In our case, the reduced form is bound more tightly since the redox potential of FAD/$FADH_2$ is elevated by 75 mV when bound to POX compared to the free cofactor. From this, the Nernst equation yields a 340-fold higher affinity of the protein to $FADH_2$ than to FAD. It is conceivable that the amino acid exchange affects the binding of the two forms of FAD to the same degree, resulting in no net change of the redox potential. But while

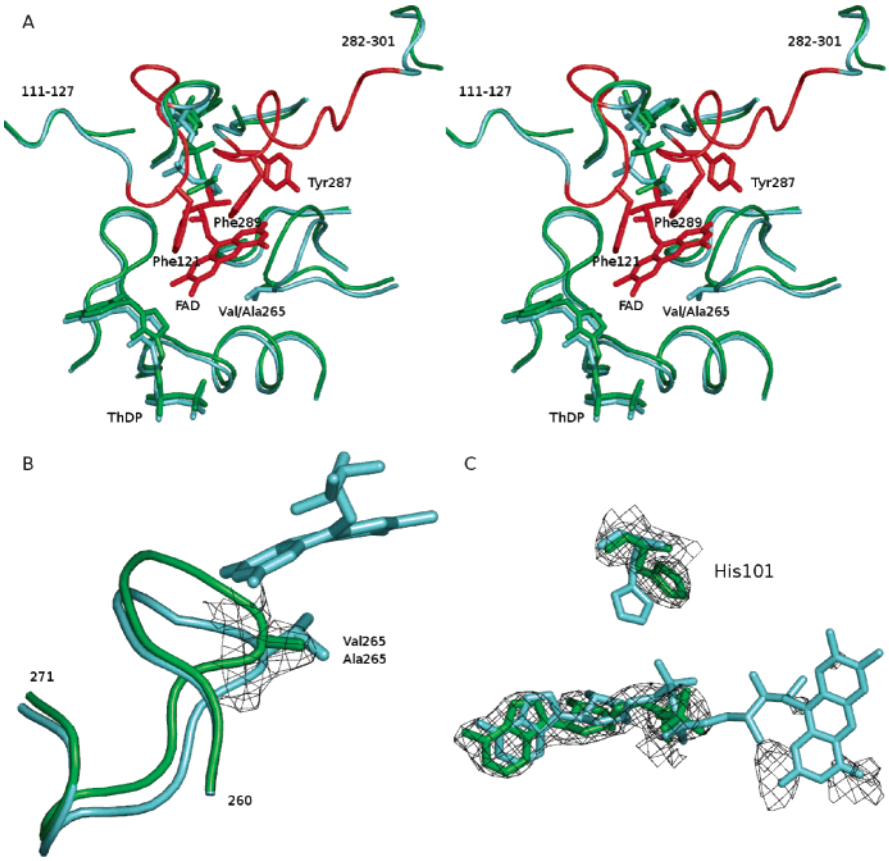

FIGURE 8: (A) Stereoview of the active sites of wild-type POX and POX-V265A. Protein loops in the vicinity of the isoalloxazine ring are given in a schematic ribbon representation. The cofactors FAD and ThDP, Val/Ala265 near the *re* face of the flavin, and the side chains of bulky aromatic residues Phe121, Tyr287, and Phe289 on the *si* face are indicated as stick models. The variant structure is in green. Wild-type structure is in cyan and red, with the red parts indicating where electron density is missing for the equivalent residues in the variant POX-V265A. (B) Loop around the mutated residue 265 in a ribbon representation of the protein backbone. Cyan color is used for the wild-type structure and green for the loop in the variant protein. While the ends of the loop (here residues 260 and 271) match well for both structures, the immediate vicinity of residue 265 shows greater deviation; the variant loop appears to be moving inward into the flavin binding site. Electron density is shown as a wire mesh around Ala265 at a σ-level of 1.0 in a $2F_o - F_c$ map. (C) FAD region in the wild-type structure (cyan) and the variant (green). Electron density shown for the structure of the variant is at a σ-level of 1.5 in the $2F_o - F_c$ map. It is well-defined for the ADP moiety (left) but lacking for the ribityl-isoalloxazine part except in the vicinity of its carbonyl groups (right). The imidazole ring of His101 is turned away from the respective wild-type position by about 90° and has lost the hydrogen bond with the FAD phosphate.

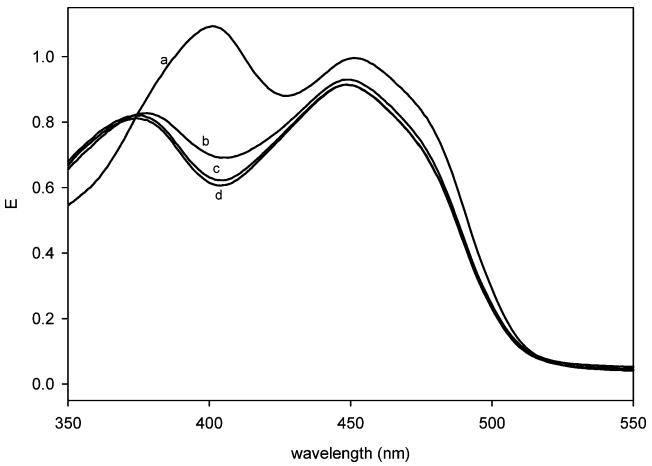

FIGURE 9: Displacement of FAD with ADP in POX-V265A (c_p = 15 mg/mL in 200 mM potassium phosphate buffer, pH 6.0). ADP concentrations are (a) 0 mM, (b) 2.8 mM, (c) 8.2 mM, and (d) 18 mM. While in spectrum a the cofactor is protein-bound, spectra c and d are spectra of almost exclusively free FAD.

the affinity for $FADH_2$ is still high enough in the variant to prevent the release of the cofactor, the binding of the oxidized form is now loose enough to release oxidized FAD into solution when the protein concentration is sufficiently low.

To test this assumption, we made use of the finding that ADP displaces FAD from the variant protein. If we added the substrate pyruvate, would the affinity of the protein for the then-reduced $FADH_2$ suffice to replace the ADP? This is indeed the case (Figure 10). When reduction of the FAD was complete after addition of pyruvate (as judged from the vis spectrum), we added oxygen to the solution by gentle stirring and acquired a spectrum immediately after all pyruvate had been depleted, and the solution had turned bright yellow again. This spectrum closely resembled the spectrum of oxidized POX-V265A *before* the addition of ADP. After several minutes, it had again turned into the ADP-displaced spectrum. We explain this curious behavior as follows: In the presence of ADP, only a fraction of active sites is complemented with FAD, as the oxidized form of the flavin is bound weakly and would be replaced by competing ADP. Addition of pyruvate eventually leads to the conversion of protein-bound FAD to $FADH_2$ because at high enzyme concentrations the molecular oxygen, which is required for the reoxidation of $FADH_2$ to FAD, cannot diffuse into the solution fast enough and becomes the limiting

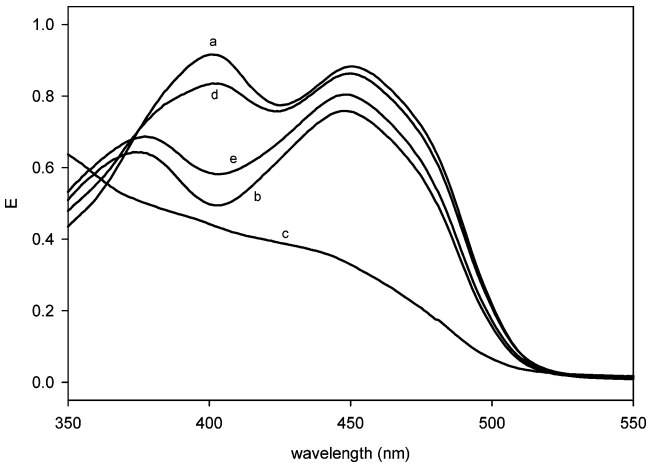

FIGURE 10: Spectra of POX-V265A in the presence of ADP during and after turnover of pyruvate. (a) Spectrum of POX-V265A (c_p ~ 12 mg/mL in 200 mM potassium phosphate, pH 6.0, and 5 mM ThDP/$MgCl_2$). (b) After addition of 9 mM ADP, the sample shows the spectrum of free FAD. (c) After further addition of 30 mM sodium pyruvate and equilibration (~30 min), all FAD has been reduced. (d) The spectrum obtained immediately after pyruvate has been depleted, and the FAD has been reoxidized; it is very similar to the spectrum of the sample before addition of ADP. Small differences result from the handling time and the time required to measure the spectrum. (e) The spectrum after an additional 7 min. The ADP in solution has once again displaced the FAD from the protein.

substrate. $FADH_2$ binds more tightly and cannot be replaced by ADP. The enzyme active sites thus become all slowly trapped in an $FADH_2$-bound state, because as soon as an ADP molecule is replaced by FAD, the latter is reduced. When addition of oxygen through stirring allows turnover to proceed and eventually all pyruvate has been consumed, reoxidized FAD is no longer being reduced to $FADH_2$. The exchange with ADP is then sufficiently slow to allow the acquisition of a vis spectrum with *oxidized* FAD bound to the protein even in the presence of ADP. After several minutes, the cofactor is once more released into the solution and the spectrum is again that of free FAD.

CONCLUSIONS

The exchange V265A in POX from *Lactobacillus plantarum* causes a number of apparently contradictory effects for the protein. The affinity for the cofactor FAD is decreased, but the catalytic activity is the same for the overall reaction, even though the electron transfer proceeds with a 3-fold lower rate than in the wild-type. This can only be due to kinetic effects, for example, an increased distance between ThDP and flavin, since the redox potential of the FAD is the same for both POX-WT and POX-V265A. Redox-triggered FTIR difference spectroscopy confirms a different binding mode of the FAD in the variant enzyme, as characteristic band shifts observed in the wild-type (compared to free FAD) are less marked (10 vs 14 cm^{-1}) for POX-V265A, arguing in favor of a more relaxed conformation.

This is confirmed by the crystal structure, which lacks interpretable electron density for the riboflavin moiety of FAD and also for two loops lining the flavin binding pocket. Residual density near the isoalloxazine carbonyl groups suggests that some hydrogen bonds which are present in the wild-type still persist in the variant. This could contribute to the remaining IR peak shift and also to the unchanged redox potential in the enzyme variant. The ADP part of the flavin is well-defined, and it is indeed possible to displace FAD from the variant enzyme with adenine nucleotides. This behavior is not without precedent. POX is peculiar with regard to cofactor binding: it does not belong to any of the three big families of FAD-binding proteins, in which each shares a common fold (glutathione reductase, ferredoxin reductase, and *p*-cresol methylhydroxylase family). Instead, it forms its own group (*33*). One of the few other members of this group is electron-transfer flavoprotein, for which Sato et al. reported that FAD binding is largely dependent on the ADP moiety of the cofactor, with the riboflavin part contributing only little to binding (*34*).

The lack of electron density for the isoalloxazine ring precludes a definitive assessment of the significance of the flavin distortion in the wild-type structure with respect to the redox potential and curious band shifts in the POX-WT IR spectrum. However, it appears that the ring is under less steric strain than in the wild-type, given the presence of local disorder and flexibility in the structure of the variant. We conclude from these findings that the flavin bend in wild-type POX is not the main reason for its increased redox potential compared to free FAD. Crystal structures of *reduced* wild-type and variant POX would greatly help in the discussion of these points, but none have been forthcoming so far.

ACKNOWLEDGMENT

We thank Prof. R. Jaenicke and Mrs. A. Jaenicke for their generous support, Prof. K. Tittmann and Dr. P. Hellwig for helpful discussions, Mr. J. Fanghänel for comments on the manuscript, and the EMBL Hamburg for the provision of beam time.

REFERENCES

1. Sedewitz, B., Schleifer, K. H., and Götz, F. (1984) Purification and biochemical characterization of pyruvate oxidase from *Lactobacillus plantarum*, *J. Bacteriol. 160*, 273−278.
2. Muller, Y. A., and Schulz, G. E. (1993) Structure of the thiamine- and flavin-dependent enzyme pyruvate oxidase, *Science 259*, 965−967.
3. Muller, Y. A., Schumacher, G., Rudolph, R., and Schulz, G. E. (1994) The refined structures of a stabilized mutant and of wild-type pyruvate oxidase from *Lactobacillus plantarum*, *J. Mol. Biol. 237*, 315−335.
4. Zheng, Y., and Ornstein, R. L. (1996) A theoretical study of the structures of flavin in different oxidation and protonation states, *J. Am. Chem. Soc. 118*, 9402−9408.
5. Rizzo, C. J. (2001) Further computational studies on the conformation of 1,5-dihydrolumiflavin, *Antioxid. Redox Signaling 3*, 737−746.
6. Wille, G., Ritter, M., Friedemann, R., Mäntele, W., and Hübner, G. (2003) Redox-triggered FTIR difference spectra of FAD in aqueous solution and bound to flavoproteins, *Biochemistry 42*, 14814−14821.
7. Massey, V., and Hemmerich, P. (1980) Active-site probes of flavoproteins, *Biochem. Soc. Trans. 8*, 246−257.
8. Hasford, J. J., Kemnitzer, W., and Rizzo, C. J. (1997) Conformational effects on flavin redox chemistry, *J. Org. Chem. 62*, 5244−5245.
9. Berman, H. M., Westbrook, J., Feng, Z., Gilliland, G., Bhat, T. N., Weissig, H., Shindyalov, I. N., and Bourne, P. E. (2000) The protein data bank, *Nucleic Acids Res. 28*, 235−242.

10. Watt, W., Tulinsky, A., Swenson, R. P., and Watenpaugh, K. D. (1991) Comparison of the crystal structures of a flavodoxin in its three oxidation states at cryogenic temperatures, *J. Mol. Biol. 218*, 195−208.
11. Binda, C., Coda, A., Angelini, R., Federico, R., Ascenzi, P., and Mattevi, A. (1999) A 30 Å long U-shaped catalytic tunnel in the crystal structure of polyamine oxidase, *Structure 7*, 265−276.
12. Binda, C., Angelini, R., Federico, R., Ascenzi, P., and Mattevi, A. (2001) Structural bases for inhibitor binding and catalysis in polyamine oxidase, *Biochemistry 40*, 2766−2776.
13. Fox, K. M., and Karplus, P. A. (1994) Old yellow enzyme at 2 Å resolution: overall structure, ligand binding, and comparison with related flavoproteins, *Structure 2*, 1089−1105.
14. Waksman, G., Krishna, T. S. R., Williams, C. H., Jr., and Kuriyan, J. (1994) Crystal structure of *Escherichia coli* thioredoxin reductase refined at 2 Å resolution. Implications for a large conformational change during catalysis, *J. Mol. Biol. 236*, 800−816.
15. Lennon, B. W., Williams, C. H., Jr., and Ludwig, M. L. (1999) Crystal structure of reduced thioredoxin reductase from *Escherichia coli*: structural flexibility in the isoalloxazine ring of the flavin adenine dinucleotide cofactor, *Protein Sci. 8*, 2366−2379.
16. Gibson, Q. H., Swoboda, B. E. P., and Massey, V. (1964) Kinetics and mechanism of action of glucose oxidase, *J. Biol. Chem. 239*, 3927−3934.
17. Moss, D., Nabedryk, E., Breton, J., and Mäntele, W. (1990) Redox-linked conformational changes in proteins detected by a combination of infrared spectroscopy and protein electrochemistry. Evaluation of the technique with cytochrome *c*, *Eur. J. Biochem. 187*, 565−572.
18. Hellwig, P., Scheide, D., Bungert, S., Mäntele, W., and Friedrich, T. (2000) FT-IR spectroscopic characterization of NADH:ubiquinone oxidoreductase (complex I) from *Escherichia coli*: oxidation of FeS cluster N2 is coupled with the protonation of an aspartate or glutamate side chain, *Biochemistry 39*, 10884−10891.
19. Otwinowski, Z., and Minor, W. (1997) Processing of X-ray diffraction data collected in oscillation mode, *Methods Enzymol. A276*, 307−326.
20. Vagin, A. A., and Teplyakov, A. (1997) MOLREP: an automated program for molecular replacement, *J. Appl. Crystallogr. 30*, 1022−1025.
21. Jones, T. A., Zou, J. Y., Cowan, S. W., and Kjeldgaard, M. (1991) Improved methods for building protein models in electron density maps and the location of errors in these models, *Acta Crystallogr. A47*, 110−119.
22. Murshudov, G. N., Vagin, A. A., and Dodson, E. J. (1997) Refinement of macromolecular structures by the maximum-likelihood method, *Acta Crystallogr. D53*, 240−255.
23. Collaborative Computational Project, Number 4 (1994) The *CCP*4 suite: programs for protein crystallography, *Acta Crystallogr. D50*, 760−763.
24. DeLano, W. L. (2002) *The PyMOL Molecular Graphics System*, DeLano Scientific, San Carlos, CA (http://www.pymol.org).
25. Risse, B., Stempfer, G., Rudolph, R., Möllering, H., and Jaenicke, R. (1992) Stability and reconstitution of pyruvate oxidase from *Lactobacillus plantarum*: dissection of the stabilizing effects of coenzyme binding and subunit interaction, *Protein Sci. 1*, 1699−1709.
26. Tittmann, K., Golbik, R., Ghisla, S., and Hübner, G. (2000) Mechanism of elementary catalytic steps of pyruvate oxidase from *Lactobacillus plantarum*, *Biochemistry 39*, 10747−10754.
27. Kuzmic, P. (1996) Program DYNAFIT for the analysis of enzyme kinetic data: application to HIV proteinase, *Anal. Biochem. 237*, 260−273.
28. Barth, A. (2000) The infrared absorption of amino acid side chains, *Prog. Biophys. Mol. Biol. 74*, 141−173.
29. Mayhew, S. G. (1999) The effects of pH and semiquinone formation on the oxidation−reduction potentials of flavin mononucleotide, *Eur. J. Biochem. 265*, 698−702.
30. Weiss, M. S. (2001) Global indicators of X-ray data quality, *J. Appl. Crystallogr. 34*, 130−135.
31. Schütz, A., Sandalova, T., Ricagno, S., Hübner, G., König, S., and Schneider, G. (2003) Crystal structure of thiamindiphosphate-dependent indolepyruvate decarboxylase from *Enterobacter cloacae*, an enzyme involved in the biosynthesis of the plant hormone indole-3-acetic acid, *Eur. J. Biochem. 270*, 2312−2321.
32. Tittmann, K., Proske, D., Spinka, M., Ghisla, S., Rudolph, R., Hübner, G., and Kern, G. (1998) Activation of thiamin diphosphate and FAD in the phosphate-dependent pyruvate oxidase from *Lactobacillus plantarum*, *J. Biol. Chem. 273*, 12929−12934.
33. Dym, O., and Eisenberg, D. (2001) Sequence-structure analysis of FAD-containing proteins, *Protein Sci. 10*, 1712−1728.
34. Sato, K., Nishina, Y., and Shiga, K. (1992) The binding of adenine nucleotides to apo-electron-transferring flavoprotein, *J. Biochem. 112*, 804−810.

BI047337O